JCIM JOURNAL OF CHEMICAL INFORMATION AND MODELING

pubs.acs.org/jcim Article

Quantum Mechanical Investigation of Three-Dimensional Activity Cliffs Using the Molecules-in-Molecules Fragmentation-Based Method

Bishnu Thapa, Jon Erickson, and Krishnan Raghavachari*

Cite This: https://dx.doi.org/10.1021/acs.jcim.9b01123 Read Online

ACCESS | Metrics & More | Article Recommendations | Supporting Information

ABSTRACT: The concept of activity cliff (AC) (i.e., a small structural modification resulting in a substantial bioactivity change) is widely encountered in medicinal chemistry during compound design. Whereas the study of ACs is of high interest as it provides a wealth of opportunities for effective drug design, its practical application in the actual drug development process has been difficult because of significant computational challenges. To provide some understanding of the ACs, we have carried out a rigorous quantum-mechanical investigation of the electronic interactions of a wide range of ACs (205 cliffs formed by 261 protein−ligand complexes covering 37 different receptor types) using multilayer molecules-in-molecules (MIM) fragmentation-based methodology. The MIM methodology enables performing accurate high-level quantum mechanical (QM) calculations at a substantially lower computational cost, while allowing for a quantitative decomposition of the protein−ligand binding energy into the contributions from individual residues, solvation, and entropy. Our investigation in this study is mainly focused on whether the QM binding energy calculation can correctly identify the higher potency cliff partner for a given ligand pair having a sufficiently high activity difference. We have also analyzed the effect of including crystal water molecules as a part of the receptor as well as the impact of ligand desolvation energy on the correct identification of the more potent ligand in a cliff pair. Our analysis reveals that, in the majority of the cases, the AC prediction could be significantly improved by carefully identifying the critical crystal water molecules, whereas the contribution from the ligand desolvation also remains essential. Additionally, we have exploited the residue-specific interaction energies provided by MIM to identify the key residues and interaction hot-spots that are responsible for the experimentally observed drastic activity changes. The results show that our MIM fragmentation-based protocol provides comprehensive interaction energy profiles that can be employed to understand the distinctiveness of ligand modifications, for potential applications in structure-based drug design.

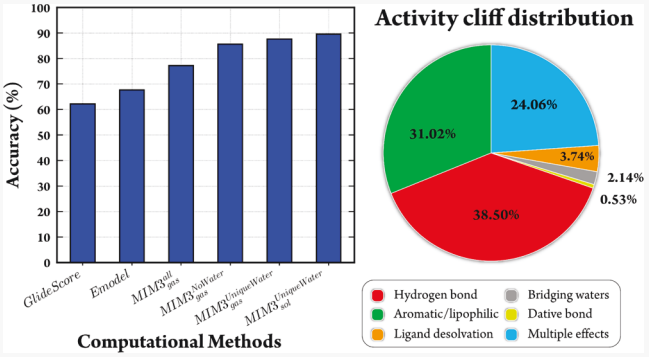

1. INTRODUCTION

The essence of drug action stems from its molecular recognition with the target receptor. As such, a complete characterization and understanding of the molecular interactions comprising the target−drug recognition is crucial for drug design. The relationship between the chemical structure of a molecule and its biological activity, also known as structure−activity relationship (SAR), has enabled the recognition of the molecular groups responsible for an observed biological effect.[1,2] An understanding of the SAR [both qualitative as well as quantitative (i.e., QSAR)] provides the key information for the modification of the chemical structure of a small molecule to enhance the desired biological effect.[1,3] The correlation between the structure of a small molecule and its bioactivity has also aided the development of various physical or empirical (statistical or machine learning) algorithms that can screen several thousands of structures to obtain a few dozen chemical compounds having the desired physicochemical and biological properties.[4−12] Although such models are used to learn from the ever-growing SAR databases and then employed to predict the potency of a new molecule, such predictions are not always reliable.[2,13] More specifically, such models perform quite poorly when a small structural change leads to a significant activity (or potency) change (>100-fold), commonly known as activity cliffs (ACs) or property cliffs.[13−20] ACs showing a dramatic effect from small structural modifications are frequently found in medicinal chemistry during compound design. In the past few years, such ACs have received significant interest in drug design from both computational and medicinal chemists because their deliberate

Received: December 3, 2019

use provides wider opportunities in lead-optimization projects.[20−22]

Although there are several distinct advantages of utilizing the ACs in drug design protocols,[20,21] practical implementation in the actual drug development process is nontrivial because it heavily relies on the accurate identification of such effects as well as their understanding. Over the years, many publications have focused on the development of new computational protocols to identify and apply the concept of ACs.[18,20,21] Mostly, the compound similarity is evaluated based on the two-dimensional (2D) molecular representation by calculating the similarity values using some molecular-graph-based descriptors such as molecular fingerprints and Tanimoto similarity coefficients.[15] The ACs can also be identified using the matched molecular pair (MMP) formalism, and its variants, in which a pair of compounds with significant activity variance differ only at specific sites represented by a substructure (such as R-group substitution on an aromatic ring).[23,24] As the ligand similarities are analyzed based on the molecular substructures, MMP can also provide a physically meaningful chemical interpretation of the ACs. A more rigorous approach to identify the AC is based on the three-dimensional (3D) structures, where a pair of bound ligands in the complex structure with a given target protein show significant spatial similarities along with a drastic activity change (3D-cliffs).[25,26]

As much as the advantage of ACs in obtaining new bioactive ligands (and ways to identify them) has been discussed in the literature, significantly less work has been done in the context of implementation to benefit the drug discovery process. The major challenge lies in the fact that most of the empirical models, including QSAR, are based on the *linear* similarity property principle, whereas ACs are inherently *nonlinear*. Furthermore, even the nonlinear models such as those based on machine learning or neural networks struggle to identify the ACs as they still rely on continuous SAR. Some of the somewhat successful but relatively new approaches to identify the ACs in a given dataset include the structure−activity landscape index,[27] MMPs,[23,24] retrosynthetic MMPs,[28] and compound−core relationship[29] formalisms. Additionally, the concept of 3D cliffs has also been used to investigate the ability of different docking and scoring approaches to identify the substantial activity change in structurally similar ligands.[25,26,30,31]

Another complication in incorporating the activity cliff information in an empirical scoring function is due to the challenges in identifying a proper, chemically intuitive, molecular descriptor. As the interactions that trigger a sudden activity change are specific to the particular receptor and the inhibitor, it is highly difficult to generalize such descriptors globally. Furthermore, when a structural change does not necessarily alter any distinct new nonbonded interaction (e.g., steric repulsion or hydrogen bond), an accurate explanation or prediction of such an AC is complicated, even for the force-field-based scoring functions that explicitly define the electrostatic and van der Waals interactions.[32,33] In contrast, quantum mechanical (QM) methods, in principle, include all contributions to the protein−ligand (P−L) interaction energies, and hence should be ideal for such studies. An appropriate high-level QM calculation could be a much-needed approach to address the deficiencies in the current scoring functions while providing a better understanding of the AC formation. Indeed, an increasing number of studies have attempted to use the free-energy-based and QM-based approaches to provide an electronic-level understanding of P−L interactions, including in the analysis of ACs.[34−38]

In this study, we have employed a high-level QM method to explore and understand the formation of ACs on a set of 205 3D-cliffs formed by 261 unique ligands reported in a previous study by Bajorath and co-workers.[25] The computational cost of the associated QM calculation is reduced using our multilayer molecules-in-molecules (MIM) fragmentation-based method.[39−41] The multilayer MIM method is capable of reproducing the total energy within 2 kcal/mol of an unfragmented full molecule.[40,41] The performance of the MIM approach is even better for calculating the interaction energies, yielding values within 1 kcal/mol of those obtained with the full, unfragmented molecule with a good correlation (R^2 = 0.98).[42] The MIM method has already been applied to analyze the P−L interactions involved in several congeneric series of inhibitors including interleukin-2-inducible T-cell kinase (ITK) inhibitors, cyclin-dependent kinase 2 (CDK2) inhibitors, and thrombin inhibitors.[41,42] Using the MIM method, we have also shown that contributions of the interactions from each amino acid residue can be analyzed more effectively using an energy decomposition scheme to identify the critical residues.[43] Such a residue-specific energy decomposition analysis could also be used to differentiate two ligands to obtain the net interaction difference, which makes the MIM an ideal method for understanding the ACs.

In the following, we present an MIM method-based approach for the investigation of the ACs present in a wide variety of receptors, including metalloproteins. In particular, we aim to reproduce the relative ordering of a large number of ACs using a high-level QM method with a proper accounting of the differential solvation effects. The role of crystal water molecules and the effect of ligand desolvation energy on AC formation has also been carefully explored. Additionally, we have exploited the residue-specific interaction energies provided by MIM to identify the key residues and interaction hot-spots that are responsible for the experimentally observed drastic activity changes. The results show that our MIM fragmentation-based protocol provides comprehensive interaction energy profiles that can be employed to understand the distinctiveness of ligand modifications, for potential applications in structure-based drug design (SBDD).

2. METHODS

2.1. Data Sets and Structure Preparation. A comprehensive set of 269 ligands bound to 37 target sets belonging to 17 different protein families forming a total of 216 3D cliffs was considered in this study. These 3D-cliffs were obtained from the Supporting Information of a remarkably rigorous study by Bajorath and co-workers.[25] In the original 3D cliff study, these authors assembled a total of 12,145 protein−ligand complexes with 2426 unique receptors from BindingDB and ChEMBL, and systematically screened to obtain 216 well-defined 3D cliffs based on the following criteria.

(a) To obtain high confidence experimental binding affinities, any complexes with uncertain binding potencies, that is, with ">" or "<" symbol, were discarded.

(b) For each target, there must be at least two complexes with experimentally measured binding affinities to be considered for the cliff formation.

(c) For a ligand pair to qualify to possess a cliff, it must have >80% 3D similarity and must have a 100-fold potency

https://dx.doi.org/10.1021/acs.jcim.9b01123
J. Chem. Inf. Model. XXXX, XXX, XXX−XXX

difference. The strongest binding partner of the cliff must have a nanomolar (nM) binding affinity (K_i) value. The similarity evaluation was performed by using a 3D similarity function with appropriate density functions, taking positional, conformational, and property differences into account.

The resulting 3D cliff set consists of 269 ligands bound to 38 target sets belonging to 17 different protein families (Table S1). The details about the screening protocol and further analysis to obtain 3D cliffs can be found in the original refs 25 and 26.

The structures of the abovementioned 269 protein−ligand complexes were downloaded from the protein data bank,[44] and further visually analyzed using the molecular operating environment (MOE) graphical interface[45] to obtain the final test set. In particular, we analyzed the structures to make sure that the crystal structure does not have an error in the ligand structure (i.e., missing or duplicated ligand atoms or bonds) compared to the ligand reported in the original experimental study. In four of the cases, we observed that the crystal structure had an erroneous ligand, that is, with parts of the ligand present at multiple places. In four additional instances, the ligands were found to form a covalent bond with the receptor. Those eight ligands were not considered for further analysis. Thus, our final dataset includes a total of 261 ligand−receptor complexes forming 205 ACs. We believe that this dataset is sufficiently large to derive several fairly definitive conclusions (*vide infra*).

Missing hydrogen atoms in the crystal structure were added with the Protonate3D[46] tool as implemented in MOE at a neutral pH of 7. Protein−ligand complexes were then energy-minimized in MOE with the AMBER10:EHT force field,[47] using a generalized Born/volume integral implicit solvation model with an internal dielectric constant of 2 for the binding pocket and an external dielectric constant of 80. The minimization was performed under a 0.5 Å restraint for every atom with respect to the starting structure. As the MM minimizations were performed on the high-resolution crystal structures (resolution < 2.5 Å) with some constraint, it is assumed that the resulting protein−ligand complexes are quite close to the correct binding modes. Therefore, they should be reliable enough for the comparative study of the pairs of structurally similar ligands (>80% 3D similarity) bound to the same receptor. Indeed, our previous studies (and also this study) have shown that this approach results in reliable structures to reproduce the experimental binding trends.[42,43]

As the calculations are performed in the gas phase, any charged ligand and all charged residues such as lysine, arginine, glutamate, and aspartate were neutralized by adding/removing protons to better match the stabilization seen in the solution. In our previous study, we have shown that this is an appropriate approximation for calculating protein−ligand interaction energies in the gas phase that correlates well with the corresponding experimental binding potencies.[42,43] To further assure that the neutralizing the charged groups does not lead to a misrepresentation of the real systems, we computed the interaction energies of a total of 46 AC pairs (total of 70 unique protein−ligand complexes) having a net difference in the ligand formal charges. A significant consistency in the results between the fully charged versus charge-neutral system further validated our approximation (see Supporting Information Table S7). For the QM calculations, all residues along with crystal water molecules present within 6.0 Å of the ligand were selected. The selected regions were then extended to include the full residues at the boundary. Our previous study has shown that including the residues within 6.0 Å of a ligand is sufficient to capture all of the most crucial residues that play a determining role in protein−ligand binding.[43] All the cut bonds were capped with hydrogen atoms to satisfy the chemical valence. The final QM region includes a total number of atoms in the range of 550−1400 depending upon the size of the ligand.

2.2. MIM Method and Fragmentation Strategies. MIM is a multilevel hybrid energy fragmentation approach similar in spirit to the ONIOM methodology developed by Morokuma and co-workers.[48] Whereas more details about the MIM method can be found in our previous publications,[39−41,48] here we provide a brief overview of the methodology adopted in this study. All QM calculations were performed using our three-layer MIM fragmentation-based method (i.e., MIM3). In MIM3, a molecule is fragmented to form three increasingly larger sized subsystems ($r \ll r' \ll R$), and the three subsystems are treated with three different levels of theory. As in our previous study, high-layer subsystems (r) are generated by forming pairs of amino acid residues or crystal waters with the ligand (Scheme 1). In the cases where the ligand is significantly large (>30 heavy atoms), the ligand is also split into multiple fragments by cutting appropriate C−C bonds to make it computationally tractable. As in our previous study,[43] the protein is divided by cutting the C−Cα and Cα−Cβ bonds, to obtain the initial nonoverlapping monomers. In this scheme, each amino acid residue is divided into two monomers, containing the backbone atoms (HC(=O)−NH−CH_3) and the side chain, respectively. Such a

Scheme 1. Illustration of the MIM Fragmentation Scheme Used in MIM2 and MIM3 Calculations[a]

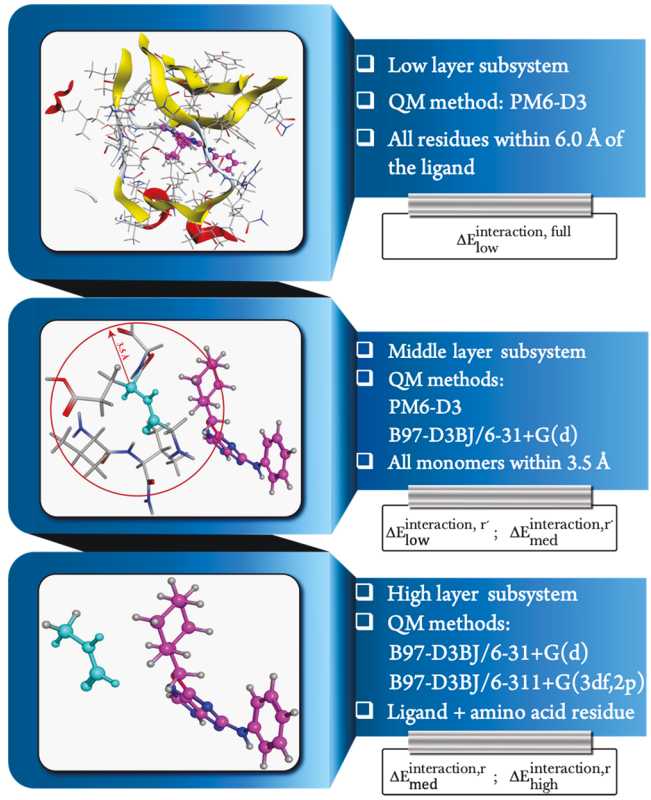

[a]All carbon atoms of the ligand are shown in pink. In high- and middle-layer subsystems, the fragment starting a subsystem is colored in cyan.

https://dx.doi.org/10.1021/acs.jcim.9b01123
J. Chem. Inf. Model. XXXX, XXX, XXX−XXX

fragmentation scheme is convenient to obtain residue-specific interaction energies (vide infra) that allows gathering a more precise quantitative information of the residues contributing significantly to the observed differences in the experimental binding affinities of a pair of ligands. As the peptide bonds between the amino acid residues have a partial double bond character and therefore are not broken during the MIM fragmentation, the definition of an amino acid residue is slightly different (i.e., 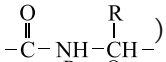) compared to the conventional structure (i.e., 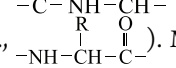). Middle-layer subsystems (r') are generated using a distance-based fragmentation scheme with a cutoff radius of 3.5 Å. In the low-layer (R), the full molecule is calculated at a computationally efficient, semiempirical method, PM6-D3. As the subsystems generated in each layer are overlapping, the overcounting of atoms is corrected by forming derivative subsystems using the *inclusion−exclusion principle*. Independent energy calculations are then performed in each layer, and the total energy is obtained by appropriate summation of the subsystem energies, as shown in eq 1.[43]

$$E^{\mathrm{MIM}} = \sum_i E^i - \sum_{i<j} E^{i\cap j} + \sum_{i<j<k} E^{i\cap j\cap k} - \ldots + (-1)^{n-1} \sum_n E^{i\cap j\cap k\cap \ldots \cap n} \quad (1)$$

Here, the first term, E^i represents the energy of the ith primary subsystem. The second and following energy terms (such as $E^{i\cap j}$, $E^{i\cap j\cap k}$) correspond to the derivative subsystems from the overlapping region between the primary subsystems formed to correct the overcounting.

The general energy expression for MIM3 can be written as

$$E^{\mathrm{MIM3}} = E^{r}_{\mathrm{high}} - (E^{r}_{\mathrm{med}} - E^{r'}_{\mathrm{med}}) - (E^{r'}_{\mathrm{low}} - E^{R}_{\mathrm{low}}) \quad (2)$$

where $r \ll r' \ll R$ are the three arbitrary fragmentation parameters used in the high, middle, and low layers. E^{r}_{high} and E^{r}_{med} are the MIM energies calculated for the high-layer (r) subsystems with the high and medium levels of theory, respectively; $E^{r'}_{\mathrm{med}}$ and $E^{r'}_{\mathrm{low}}$ are the MIM energies calculated for the middle-layer (r') subsystems with the medium and low levels of theory, respectively, and E^{R}_{low} is the total energy calculated for the low-layer (R) subsystems at the low level of theory.

The interaction energy between a protein and a ligand in a P−L complex can be calculated as

$$E^{\mathrm{interaction}} = E^{\mathrm{complex}} - E^{\mathrm{protein}} - E^{\mathrm{ligand}} \quad (3)$$

Here, E^{complex}, E^{complex}, and E^{complex} are the total energy of a P−L complex, a protein, and a ligand, respectively, which can be calculated individually using eq 2.

As the interaction energy between the protein and the ligand of a P−L complex is calculated by separating them at an infinite distance without changing their coordinates, it is possible to have some identical subsystems formed for the complex as well as the protein due to the MIM fragmentation. As the energy contribution from those subsystems will eventually cancel out and therefore will not contribute to the calculated total interaction energy, the energy calculation of those subsystems can be avoided to further lower the computational cost without compromising the accuracy. Therefore, for a given protein−ligand complex, instead of separately calculating the total MIM3 energies for a PL complex, a protein, and a ligand using the eq 2 and subtracting them later (eq 3), the total interaction energy for a molecule using our three-layer MIM is directly calculated as

$$\Delta E^{\mathrm{interaction}}_{\mathrm{MIM3}} = \Delta E^{\mathrm{interaction},r}_{\mathrm{high}} - (\Delta E^{\mathrm{interaction},r}_{\mathrm{med}} - \Delta E^{\mathrm{interaction},r'}_{\mathrm{med}}) - (\Delta E^{\mathrm{interaction},r'}_{\mathrm{low}} - \Delta E^{\mathrm{interaction,full}}_{\mathrm{low}}) \quad (4)$$

where $\Delta E^{\mathrm{interaction},r}_{\mathrm{high}}$ and $\Delta E^{\mathrm{interaction},r}_{\mathrm{med}}$ are the total interaction energies calculated for the residue−ligand pairs with the high and medium levels of theory, respectively; $\Delta E^{\mathrm{interaction},r'}_{\mathrm{med}}$ and $\Delta E^{\mathrm{interaction},r'}_{\mathrm{low}}$ are the total interaction energies calculated with medium and low levels of theories with the distance-based fragmentation scheme, and $\Delta E^{\mathrm{interaction,full}}_{\mathrm{low}}$ is the total interaction energy calculated for the full molecule at the low level of theory.

Each of the $\Delta E^{\mathrm{interaction}}$ terms in eq 4 is calculated as

$$\Delta E^{\mathrm{interaction}}_{\mathrm{high/mid/low}} = \sum_k^N \Delta E^{k}_{\mathrm{high/mid/low}} \quad (5)$$

Here, N is the number of subsystems formed in the high, middle, and low layers, and ΔE^k is the interaction energy of the kth subsystem.

As the high-layer fragments involve residue−ligand pairs, the total protein−ligand interaction energy calculated using MIM3 can be partitioned into residue-specific interactions at the high level of theory. However, as the residue-specific interaction energies calculated only at the high layer will not add up to the total MIM3 interaction energy because of the missing many-body effects, we use a single uniform scaling factor to correct the per-residue interactions. This scaling factor (α) is obtained from the ratio of the total interaction energy ($\Delta E^{\mathrm{interaction}}_{\mathrm{MIM3}}$) and the sum of the per-residue interaction energies calculated at the high layer ($\Delta E^{\mathrm{interaction},r}_{\mathrm{high}}$), as shown in eq 4. This approach has been carefully calibrated in our recent study[43] and shown to be reasonably accurate to study the relative strength of residue-specific interactions of structurally similar ligands as investigated in this study.

$$\text{Scaling factor } (\alpha) = \frac{\Delta E^{\mathrm{interaction}}_{\mathrm{MIM3}}}{\Delta E^{\mathrm{interaction},r}_{\mathrm{high}}} \quad (6)$$

where $\Delta E^{\mathrm{interaction},r}_{\mathrm{high}} = \sum_k^N \Delta E^{k}_{\mathrm{high}}$ in which N is the number of ligand−residue pairs formed in the high layer and $\Delta E^{k}_{\mathrm{high}}$ is the interaction energy of the kth residue−ligand pair.

For all the light main group elements (i.e., H, C, N, O, F, P, S, and Cl), we have employed the B97-D3BJ method (i.e., B97[49,50] density functional with Grimme's D3 dispersion correction[51] and Becke−Johnson damping[52]) with 6-311++G(3d,2p)[53−56] basis set as a "high" level and 6-31+G(d) basis set as a "medium" level of theory. For the heavier elements or transition metals such as Br, I, Zn, and Mn, the energies are calculated at B97-D3/def2-TZVPP,[57] SDD[58] as the "high" level and B97-D3/def2-SVPP, SDD as the "medium" level of theory, both used with the SDD pseudopotential. PM6-D3[59] was used as a "low" level of theory for all atoms. Solvation effects on the interaction energy were approximated using the scaled ligand desolvation energy calculated using SMD[60] implicit solvation and the B97-D3BJ/6-311++G(3df,2p) method in conjunction with the solvent accessible surface area (SASA) as described in our previous study[42] (see Supporting Information, Section S1 for details). This approach provides a cost-effective way of approximating the solvation energy penalty of protein−ligand binding and is particularly appropriate for the comparative studies where the

https://dx.doi.org/10.1021/acs.jcim.9b01123
J. Chem. Inf. Model. XXXX, XXX, XXX−XXX

goal is to obtain the relative binding trend. However, for proper calculation of the absolute binding energy that is comparable with the experiment, a more rigorous calculation of protein−ligand interaction in solution will be necessary.

For some selected cases (vide infra), the full solvation energy of binding has been calculated using the SMD implicit solvation model and B97-D3BJ/6-31+G(d) level of theory on the full, unfragmented molecule and added to the gas-phase total MIM3 interaction energies. It is important to note that as the SMD implicit solvation model is parametrized with Hartree-Fock (HF) and density functional theory (DFT) methods, the accuracy of the calculated solvation energies is unknown for the semiempirical methods. Therefore, the semiempirical methods cannot be used for the solvation energy calculations. Furthermore, as the SMD implicit solvation model was developed mainly to study small molecules, its direct application with the default setting and uniform dielectric constant may not be appropriate for the large and irregularly shaped molecules like proteins. Even for the small molecules, it has been shown in some recent studies that the SMD solvation model has some problems, particularly in dealing with charged molecules.[60−62] Therefore, a more rigorous benchmarking of SMD implicit solvation is necessary to study the larger molecules.

Additionally, for a total of 46 AC pairs (70 unique protein−ligand complexes) having a net formal charge difference, we also computed the interaction energies directly in the aqueous solution using the MIM2 protocol with SMD/B97-D3BJ/6-311++G(3df,2p) as a high level and SMD/B97-D3BJ/6-31+G(d) as a low level of theory. The high-layer fragmentation in this MIM2 protocol is the same as the one described in the MIM3 calculation above. The MIM2 interaction energy is calculated as

$$\Delta E_{\mathrm{MIM2}}^{\mathrm{interaction}} = \Delta E_{\mathrm{high}}^{\mathrm{interaction},r} - \Delta E_{\mathrm{low}}^{\mathrm{interaction},r} + \Delta E_{\mathrm{low}}^{\mathrm{interaction,full}}) \quad (7)$$

The MIM fragmentation was performed using an in-house Perl external module, and all electronic structure calculations were performed using the Gaussian16 program suite.[63]

2.3. GlideScore. To provide a comparative assessment of the relative MIM3 calculated interaction energies, a standard evaluation of the ligand binding energies, often utilized in SBDD, was also carried out. Specifically, the Glide docking algorithm was used to estimate the protein−ligand interaction energies utilizing the Glide scoring function.[64−67] GlideScore is an empirical scoring function to estimate ligand binding free energy and includes force field (electrostatic, van der Waals) and other parameters that penalize or reward interactions that influence ligand binding. It has been refined to maximize docking accuracy and binding affinity prediction. In addition, another scoring term, EModel, was also included for a comparison. The Emodel score, typically used for selecting docking poses, weighs the force field components, that is, electrostatic and van der Waals energies, higher. In docking, Glide uses Emodel to pose selection and then ranks the best conformer against one another with GlideScore. Emodel is a combination of a modified version of GlideScore, the internal ligand strain (Einternal), and the Coulomb and van der Waals energy, but the exact formula is proprietary and not published. For each of the 261 complex X-ray structures, the protein preparation tool in Maestro was used to prepare each of the complex structures starting with the identical files used in the MIM3 calculations, followed by creation of the Glide docking grid using the ligand in each complex structure to define the position and extents of the grid using the default options.[68,69] Following the protein preparation and grid generation, Glide was used to score each ligand in the context of its protein complex, allowing the ligand to minimize in the site according to the Glide "refine in place" protocol. This procedure uses the input ligand coordinates to perform an optimization of the ligand structure in the field of the receptor, and then the ligand is scored. The goal of this docking method is to find the best-scoring pose that is geometrically similar to the input pose. The GlideScore obtained was used directly to compare to the MIM3 interaction energies and the experimental binding affinities (*vide infra*).

3. RESULTS AND DISCUSSION

In this study, we have investigated a set of 261 unique ligands, forming a total of 205 3D ACs across 37 different receptors from 17 protein families to provide a quantitative understanding of protein−ligand interactions. As mentioned earlier, the dataset was taken from a previous study by Bajorath and co-workers on a rigorous identification and classification of the 3D cliffs (*vide supra*).[25] The QM calculations are performed at the B97-D3BJ/6-311++G(3df,2p) level of theory using our MIM3 fragmentation-based protocol to reduce the computational cost. All the interaction energies are calculated in the gas phase using the restraint-minimized geometries. The solvation energy contribution to the binding energy is approximated by including only the ligand desolvation energy (see the Supporting Information Table S3 for details). As the MIM3 calculation also gives the interaction energy separately for each of the considered amino-acid residues, we have exploited those residue-specific interaction energies to further identify the source of the experimentally observed difference in binding potency for the cliff pairs. We have also explored in detail the interaction energy contribution from crystal water molecules to the total binding energy to elucidate their role in the AC formation.

We note a few important factors before presenting our results. As the interaction energies are obtained in the gas phase, the calculated values are significantly overestimated compared to the experiments because of the missing screening effect from the solvent as well as other factors such as protein and ligand reorganization energies, and error in the accuracy of the QM method [such as the accuracy of the method, basis set superposition error (BSSE), etc.]. In this study, we did not attempt to obtain the absolute binding energy differences, although some calibrated scaling factors could be employed to obtain binding energy values that are directly comparable to the experiments. Nonetheless, as the primary goal of our study is to be able to identify the more potent ligand in an AC, we mainly focused on the relative ordering of the ligands based on their interaction energies. Given the high structural similarity (>80%) in the cliff ligand pairs, we expect that the effect of excluding some of the environmental effects on the relative ligand order should be small. Indeed, at the DFT level of theory noted above, MIM correctly predicted the ligand potency ordering (i.e., larger binding energy for the more potent ligand of the AC pairs) in 77.6% of the cases (159 out of 205 AC pairs). Although this is quite respectable, we now discuss additional factors that can yield further improvement.

3.1. Role of Crystal Water Molecules. Water plays a fundamental role in protein folding, structure, and function and thus the treatment of water and specifically crystallographic water molecules is important in SBDD. Many methods have

https://dx.doi.org/10.1021/acs.jcim.9b01123
J. Chem. Inf. Model. XXXX, XXX, XXX−XXX

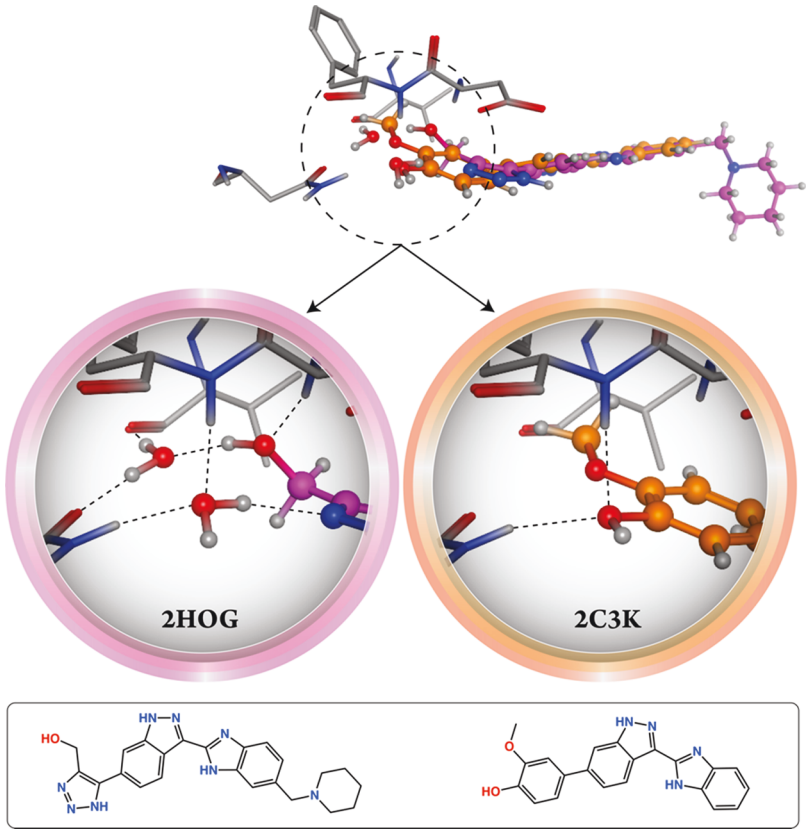

Figure 1. Illustration of the difference in the hydrogen bond formation by crystal water molecules in a pair of serine/threonine-protein kinase chk1 inhibitors resulting in an AC. The rectangular box at the bottom shows the 2D structure of the ligands.

been developed to handle water computationally to help understand their role in ligand binding.[70] The effect of water on ligand binding has been treated explicitly and with continuum methods. In this work, we considered explicit as well as implicit approaches, that is, retaining the crystal water molecules present near the ligand-binding pocket considering them as a part of the receptor, and removing them and treating the system with and without a solvent model.

To investigate the role played by crystal waters in AC formation, we computed the interaction energies with and without the contribution from those molecules and compared them with the experimental results. As mentioned above, when the crystal water molecules were considered as a part of the receptor (as in our starting point), MIM correctly predicted the ligand potency ordering in 77.6% of the cases. Most interestingly, the removal of the interaction energy contribution from crystal waters (by removing all the crystal waters from the structure) substantially improves the results: the accuracy increases from 77.6 to 86.3% (now 177 out of 205).

Such a surprising observation leads to the next question: does this mean the contribution from the explicit waters can be ignored entirely? Comparing the results with and without crystal water contributions (77.6 vs 86.3% accurate) suggests that removing the crystal waters gives overall better results. However, we do not expect that such an improvement will be consistently seen for all investigated cliffs. In fact, the relative ordering of the ligands in cliff-pairs did not change in 176 of 205 cases upon the removal of the contributions from crystal water molecules, although the total interaction energy changed quite substantially. Of the 29 cases where the relative ligand ordering changed, removing the contribution from all crystal waters leads to the correct cliff ordering in 23 cases. In the remaining six cliff pairs, removal of the contribution from explicit water molecules worsened the results. This suggests that there are some cases where having crystal water is essential for the AC formation. One such example is shown in Figure 1, where two crystal waters occupy the binding pocket of serine/threonine-protein kinase and form two strong water-mediated hydrogen bonds (−3.5 and −4.0 kcal/mol contributions). In its cliff partner, this pocket is occupied by −OH and $-OCH_3$ moieties. As expected, the contribution of the two waters in the former is found to be a key factor for the cliff formation, and therefore, they should be considered as a part of the receptor.

The existence of essential water molecules have been studied experimentally, particularly by Mattos, revealing cases where crystallographic water molecules are conserved over several X-ray structures of the same protein.[71] Here, we analyzed cases in AC pairs involving crystallographic waters and found that within 6 Å of ligand, there are as many as 16 crystal water molecules, several of which are not present in one or the other of the AC partners. Because of the significant difference in the number of explicit water molecules in the cliff partners, the resulting interaction energy contributions from crystal water molecules are found to be significantly different (see Supporting Information, Table S2 for details). Their total interaction energy contribution is also quite substantial: up to −40 kcal/mol. Therefore, the remarkable improvement in AC prediction while excluding the crystal waters can be attributed mainly to the discrepancy in the number of crystal water molecules present in the crystal structures of the cliff pair. This suggests that having an unequal number of explicit water molecules between a cliff pair is clearly not optimal for calculating the interaction energy

https://dx.doi.org/10.1021/acs.jcim.9b01123
J. Chem. Inf. Model. XXXX, XXX, XXX−XXX

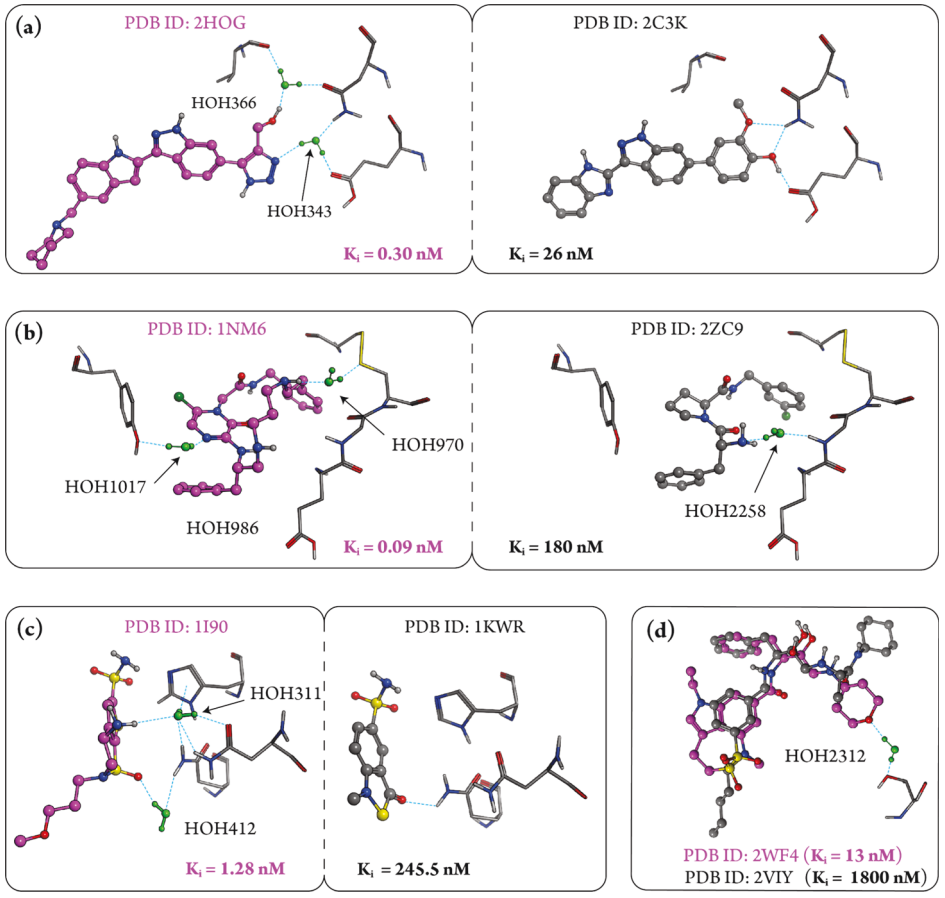

Figure 2. Water-assisted AC formation. All carbon atoms of the most potent ligand of the AC pair are shown in pink. Crystal water molecules that are unique to the specified ligand are shown in green. Only the polar hydrogens are shown for clarity. (a) Transferase-serine/threonine-protein kinase inhibitors, (b) coagulation factor II inhibitors, (c) carbonic anhydrase2 inhibitors, and (d) beta-secretase1 inhibitors.

differences. However, the uniform removal of the contribution from explicit water molecules is also not a reasonable solution because, as discussed above, it can potentially lead to incorrect predictions.

To appropriately treat the binding energy contribution from crystal water molecules, we carefully examined the crystal structures to identify the water molecules that are unique to the ligands in a cliff pair under consideration. These essential crystal waters were identified based on the following two criteria:

(a) The crystal water should form at least two hydrogen bonds, one with the ligand atoms and another with the protein. Electronegative atoms such as N, O, S, and halogens (F, Cl, Br, and I) are considered as the hydrogen bond acceptor groups. Only polar hydrogens (NH, OH, SH, PH) are considered as proton donors, and

(b) Hydrogen bonds are defined based on the donor−acceptor distance (<3.0 Å) and the angle (>130°). A crystal water molecule is considered to be unique to a ligand only if similar hydrogen bonding is not possible for its cliff partner (e.g., absence of OH group or N vs O hydrogen bond).

With the interaction energy contributions only from the unique and essential crystal water molecules fulfilling the abovementioned two criteria included, the accuracy improved further, with 88.8% of correct assignment of the most potent ligand. Compared to the results with no crystal waters included, interaction energy contribution from critical water molecules resulted in a correct assignment of cliff ordering in four cases, as shown in Figure 2.

3.2. Role of Ligand Desolvation Energy. As in our previous studies, the contribution from desolvation effects was approximated by using ligand desolvation energy calculated at the B97-D3BJ/6-311++G(3df,2p) level with SMD implicit solvation in conjunction with a model involving the SASA (see Supporting Information Section S1 for details). The contribution of ligand desolvation energy ranges from 5 to 41 kcal/mol, depending upon the size and polarity of the ligand and its contact with the bulk solvent in the bound state. The relative desolvation penalty for the cliff pairs is calculated to be in a range of +11 to −17 kcal/mol (see Table S3 for details). Although the desolvation energy contribution is quite significant, in the majority of the cases, it did not change the overall ligand ordering in the AC, that is, the strongly bound ligand in the gas phase remained the stronger one even after the addition of ligand desolvation energy difference. Only for nine of the cliff pairs shown in Table 1, the addition of ligand desolvation energy altered the relative ordering of the AC. In seven of those cases, the addition of ligand desolvation led to the correct cliff prediction. In the remaining two cases, the desolvation energy resulted in the incorrect assignment of the most potent ligand of the cliff pairs, which are discussed later in Section 3.5.

In general, the presence of polar groups in a ligand is expected to form stronger interactions such as hydrogen bond or ionic interactions with the receptor if a suitable group of a residue is present nearby. At the same time, the desolvation penalty of such

https://dx.doi.org/10.1021/acs.jcim.9b01123
J. Chem. Inf. Model. XXXX, XXX, XXX−XXX

Table 1. Ligand Pairs With Activity Cliff Order Changed with the Ligand Desolvation Energy[a]

S.N.	Ligand-1	Ligand-2	Calculated Energies (kcal/mol) $\Delta\Delta G_{experiment}$	$\Delta\Delta E_{gas}$	$\Delta\Delta E_{desolv}$	$\Delta\Delta E_{gas} + \Delta\Delta E_{desolv}$
(a) improved by ligand desolvation energy						
1.	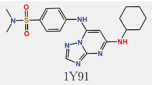 1Y91	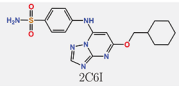 2C6I	−3.10	7.41	−8.20	−0.79
2.	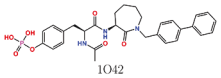 1O42	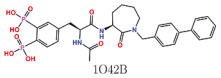 1O42B	−3.20	0.85	−4.31	−3.46
3.	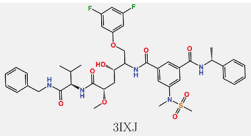 3IXJ	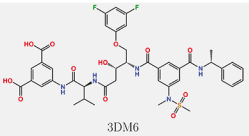 3DM6	−2.81	7.53	−11.15	−3.62
4.	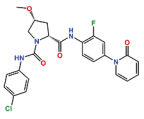 2PHB	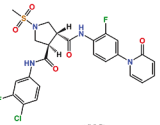 2XC5	−3.12	3.48	−4.24	−0.76
5.	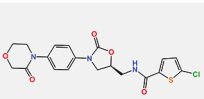 2W26	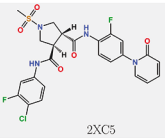 2XC5	−2.99	3.19	−5.61	−2.42
6.	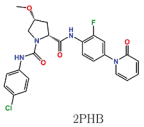 2PHB	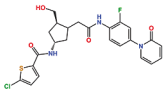 2VWL	−3.37	3.41	−3.90	−0.49
7.	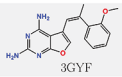 3GYF	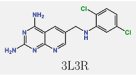 3L3R	−3.75	4.35	−7.29	−2.94
(b) worsened by ligand desolvation energy						
8.	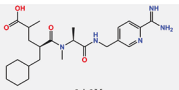 2A2X	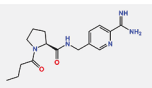 2ZI2	−5.92	−7.53	10.59	3.06
9.	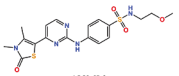 2XMY	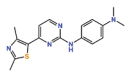 1PXP	−4.50	−9.07	10.45	1.38
10.	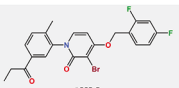 3HLL	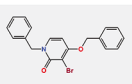 3HP2	−2.91	−3.53	5.07	1.54

[a]All values are given in kcal/mol.

a polar ligand tends to be relatively large because of its higher solubility in the aqueous medium. A closer look at the crystal structure and residue-specific interaction energies of those nine cases suggests that, in many of those cases, the ligands modified with more polar groups did not directly interact (i.e., did not form H-bond or $\pi-\pi$ stacking interactions, e.g.) with the protein. This resulted in no significant improvement in total interaction energy, though the larger desolvation energy penalty resulted in an overall lower binding affinity. For example, in a BACE1 inhibitor pair, 3IXJ and 3DM6 (ligand pair 3 in Table 1), the major difference between those two ligands is the presence of two −COOH groups and the absence of a methoxy group in the second ligand (3DM6) compared to the first (3IXJ), which results in a significant desolvation energy difference ($\Delta\Delta E_{desolv}$ = +11.15 kcal/mol) but a smaller gas-phase interaction energy advantage ($\Delta\Delta E_{gas}^{interaction}$ = −7.53 kcal/mol). A similar noticeable correlation between the polar groups and energy differences can also be observed in other cases listed in Table 1, although the desolvation energy difference is not as significant as in the BACE1 inhibitors. Overall, the inclusion of ligand desolvation improved the cliff prediction results from 88.8% in the gas phase to 91.2% in solution.

3.3. Distribution of Cliff Categories. Although, in principle, it could be possible to qualitatively categorize the ligand pairs based on the presence or absence of some specific interactions such as H-bond donor or $\pi-\pi$ interactions, the overall effect of ligand modifications involves a significantly larger number of residues than one would typically expect in small ligand modifications (see below). In many cases, we observed that a small change in ligand results in a significant shift in its position and consequently affecting a large number of residues that are not necessarily located at the actual site of ligand modification. In other cases, the effect of ligand modification is at the electronic level with a negligible

https://dx.doi.org/10.1021/acs.jcim.9b01123
J. Chem. Inf. Model. XXXX, XXX, XXX−XXX

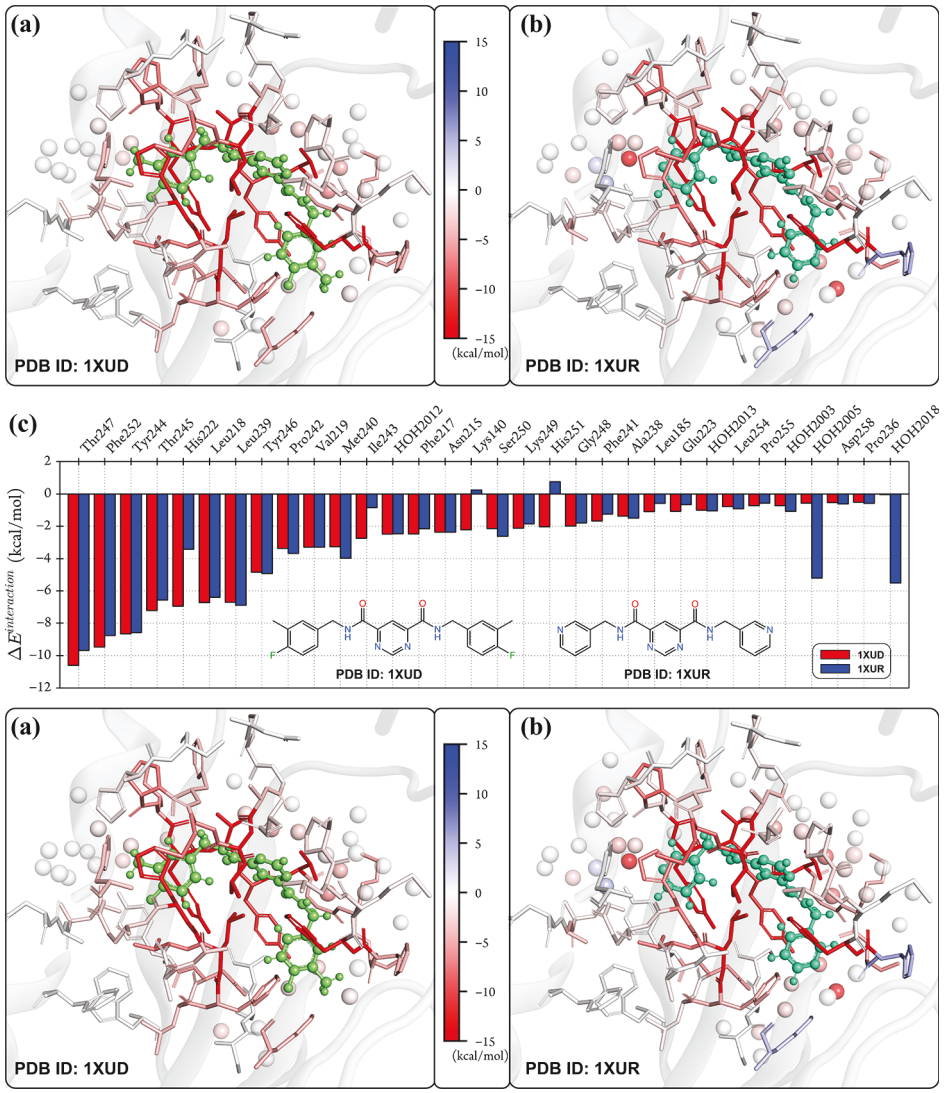

Figure 3. Residue-specific energy decomposition analysis of a pair of collagenase protein inhibitors. All residues in (a,b,d) are color-coded with red color being attractive and blue color being repulsive interactions. (c) Shows the MIM calculated residue-specific interaction energies of some select residues with contribution more than |±0.5| kcal/mol. (d,e) Show the MIM difference energy analysis (MIM-DEA) where the per-residue interactions of 1XUR are subtracted from 1XUD to obtain the relative interaction energy difference (only the residues contributing more than |±0.4| kcal/mol are shown for clarity).

geometrical change but a significant change in interaction energy [Cl (in 3E97) versus H (in 3EKR), e.g.)]. Identification of the residues playing crucial roles in the AC formation can be useful to understand the reasons for the experimentally observed significant activity change and can potentially be used in designing a new ligand.

To quantitatively identify the residues that are directly affected by the ligand modification in the 3D-cliff pairs, we have performed the MIM-difference energy analysis (MIM-DEA). In MIM-DEA, the total interaction energy calculated for a ligand using MIM3 is decomposed into the residue-specific interactions, and differences in the per-residue interaction energy are calculated for the ligand pair of interest to identify the residues affected by the ligand modification. An illustrative example is shown in Figure 3, where the quantitative information about the residue-specific interactions and the net interaction energy change for the residues that are affected by the ligand modifications are shown for a pair of collagenase inhibitors. Such residue-specific difference energy analysis provides quantitative information about the residues that interact differently for a ligand pair.

To further assist in rationalizing the residue-specific interaction energy differences into the chemical nature of the intermolecular interaction (i.e., H-bond, $\pi\cdots\pi$, C−H···H−C interactions), we also performed symmetry adapted perturbative theory (SAPT) calculations on the high-layer subsystems at the SAPT(0)/jun-cc-pVDZ level.[72] SAPT energy calculation provides a further decomposition of the residue-specific interaction into the physically meaningful components, namely: electrostatic, exchange-repulsion, polarization, and dispersion interactions.[73] Additionally, the SAPT analysis was further rationalized by careful visual inspection of the residue−aligned and superimposed protein−ligand complex geometries of the ligand pairs.

Based on the calculated interaction energy differences obtained from the residue-specific pairwise difference energy analysis augmented with SAPT energy decomposition and careful visual inspection, we have grouped the ACs into six

https://dx.doi.org/10.1021/acs.jcim.9b01123
J. Chem. Inf. Model. XXXX, XXX, XXX−XXX

categories, namely, (1) hydrogen bond, (2) aromatic/lipophilic interaction, (3) dative bond, (4) bridging water molecule, (5) ligand desolvation energy, and (6) multiple effects (Table 2).

Table 2. Distribution of Cliff Categories[a]

s. no.	cliff categories	number of target sets	number of 3D cliffs
1	hydrogen bond	23	72
2	aromatic/lipophilic interaction	23	58
3	dative bond	1	1
4	multiple effects	16	45
5	bridging water molecules	5	4
6	ligand desolvation energy	5	7

[a]The numbers of 3D cliffs is the total number of cliffs that meet both of the two criteria discussed in the text.

The residues involved in the classification are identified based on the following two energetic criteria: (1) difference in residue−ligand interaction energy ($\Delta\Delta E_{\text{pairwise}}^{\text{interaction}}$) must be larger than |±1| kcal/mol and (2) interaction energy for a type of interaction must exceed 60% of the calculated total interaction energy differences. The distribution of the energetic contributions from various interaction types for the selected ACs is depicted in Figure 4, along with the number of contributing residues. The number of 3D cliffs that fall into different categories is given in Table 2.

Our QM-assisted analysis found a total of 72 cliff pairs that are formed as a result of better hydrogen-bonding/ionic interactions. Among those 72 cliff pairs, we found 44 cliffs that are formed because of the classical hydrogen bonding (i.e., hydrogen bonding between O/N/S and NH/OH/SH groups). Six of the hydrogen bond cliffs are found to be mainly dominated by the nonclassical hydrogen bonds such as O···H−C, N···H−C, or S···H−C, and the rest of the cliffs are formed by contributions from both classical and nonclassical hydrogen bonding interactions. In 58 of the 3D-cliff pairs, the AC formation is dominated by the lipophilic interaction between the ligand and the receptor. In 33 of those cases, the cliff formation was purely due to the difference in the π interactions, which include $\pi\cdots\pi$ and $\pi\cdots$H type interactions. We also found three cases where the cliffs were formed purely by C−H···H−C type interactions, whereas the remainder were formed by the contribution from the mixture of aromatic/lipophilic interactions. In 45 of the cases, we found that multiple effects from both polar and nonpolar interactions were responsible for the observed AC formation. Interestingly, in eight of those cases, the interaction energy contribution from only the residues meeting the abovementioned criteria was not enough to result in the correct cliff assignment. This suggests that the AC formation in those cases is much more delocalized over a relatively large number of residues. Additionally, four of the ACs were formed by the bridging water molecules (Figure 2), whereas the ligand desolvation energy was found to be crucial in seven cases (Table 1), as discussed above.

3.4. Comparison of MIM Results with Glide Scores. To put the QM cliff identification results in perspective, we compared our MIM-assisted QM calculation results with Schrodinger's GlideScore, one of the most commonly used ligand screening tools in SBDD. Figure 5 summarizes the results obtained from the MIM and the GlideScore. Using the standard protocol (see the Methods section for details), GlideScore Emodel correctly identified the most potent ligand for 67.8% (139 out of 205) of the cases. MIM results, on the other hand, made correct predictions in 77.6% of the cases when the

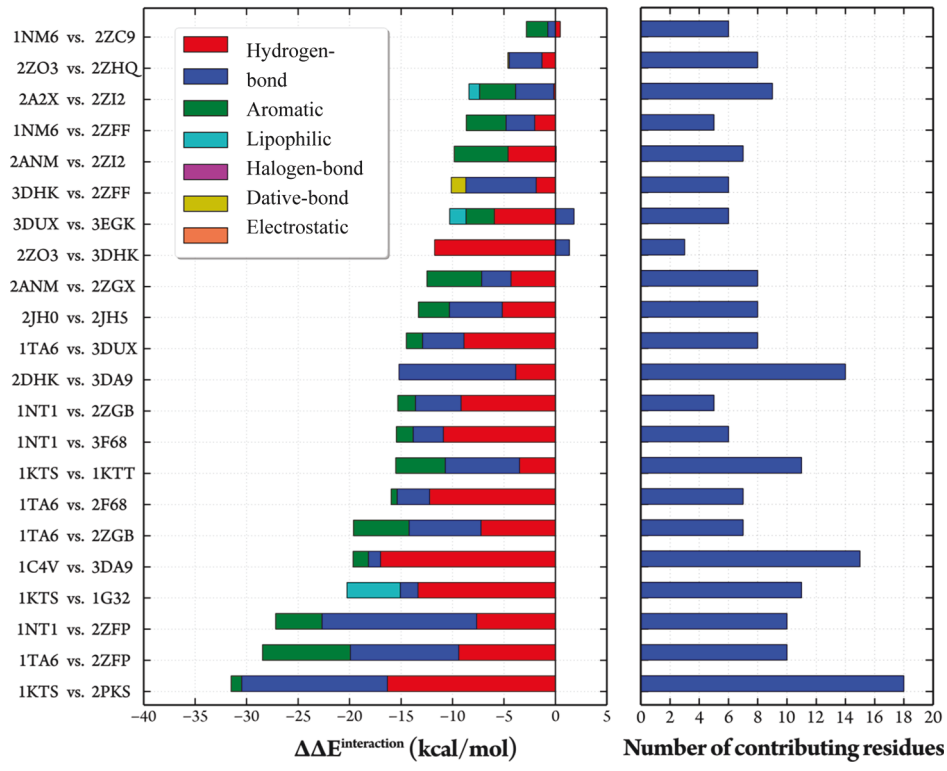

Figure 4. Illustrative example of energy contribution from various interaction types to the relative interaction energy difference calculated for the thrombin inhibitor cliff pairs. The histogram on the right shows the number of residues involved. PDB IDs of the AC pairs are shown along the *y*-axis.

https://dx.doi.org/10.1021/acs.jcim.9b01123
J. Chem. Inf. Model. XXXX, XXX, XXX−XXX

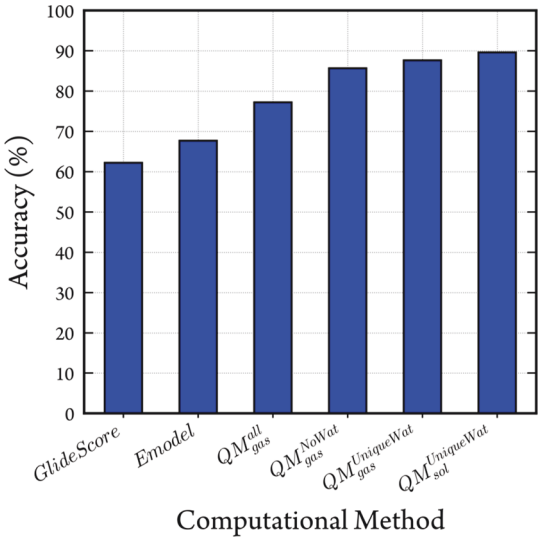

Figure 5. Comparison of the ACs prediction accuracy for various computational approaches. On the *x*-axis, the bars corresponding to QM^{all}_{gas}, QM^{NoWat}_{gas}, and $QM^{UniqueWat}_{gas}$ represent the results from MIM3 gas-phase calculation, including all atoms, excluding water molecules, and including only the unique water molecules, respectively. The rightmost bar corresponding to $QM^{UniqueWat}_{sol}$ shows the MIM3 gas-phase results plus the ligand desolvation energy.

restraint minimized X-ray crystal structures were used. As discussed above, the MIM prediction is dramatically improved to 91.2% (187 out of 205), when the interaction energies are calculated including the contributions from unique crystal water molecules and ligand desolvation energies.

Of the total 187 ACs that are correctly assigned by MIM, GlideScore assigns false-positives in 52 cases. To see if there is any specific type of interaction that is consistently underestimated by the GlideScore, we separated the cases where MIM and GlideScore results differ. Interestingly, in five of those cases, MIM identifies ligand desolvation energy as the primary contributor in the cliff formation. In 18 cases, we found that the aromatic/lipophilic interactions played the defining role in the AC formation, which is interestingly one-third of the total cliffs formed by the lipophilic interactions (total of 55 cases, Table 2). A closer inspection of the other 16 cases, where hydrogen bonding interaction was the major contributor, revealed that the nonclassical hydrogen bonding interaction (e.g., C−H···O, C−H···S) contributed significantly. Furthermore, in 13 additional cases, MIM energy decomposition analysis showed that the cliff formation arose from many smaller contributions (from 7 to 15 residues) with no single dominant interaction type. Some of the representative examples are shown in Figure 6. This analysis suggests that the relatively larger errors seen in the GlideScore are the cases where the interactions are not well-defined, that is, interactions that are dominated by the nonclassical hydrogen bonds, and lipophilic interactions involving π···H and C−H···H−C interactions. However, there is no single type of interaction that is found to be consistently underestimated in GlideScore.

Nevertheless, given the qualitative and rapid nature of the GlideScore that can scan several millions of drug structures in a few hours, it is important to note that the 67.8% accuracy obtained using the GlideScore is very good. However, in the context of how these results can be applied to the real drug design problem to narrow down the search and identification of potential drug candidates, the extra cost of carrying out the more expensive MIM-assisted QM calculations to improve results by >20% could make a big difference. Moreover, as discussed above, the quantitative per-residue energy decomposition provided by our approach can be useful in the informed drug design protocols.

3.5. Problematic Cases: Is Accurate Interaction Energy Calculation Enough? It is quite exciting to see that the QM calculated interaction energies correctly predicted the more potent ligand in a large number of ACs investigated in this study (91.2% accurate cliff assignments). However, it is equally useful to understand the cases where the high-level QM results predicted the incorrect ligand pair ordering despite having a significant experimental binding potency difference (>100-fold; <−2.5 kcal/mol). To understand the possible reason for the inability of QM calculations in predicting the relative ordering, we further analyzed the structures and energetics by including some of the other components of protein−ligand binding that are not included in our current protocol. In the interaction calculation protocol used above, we have only included two (i.e., interaction energy and ligand desolvation energy) of the many other factors that could influence the protein−ligand binding process such as protein desolvation, and vibrational and conformational entropy changes. Furthermore, it is also possible that the crystal structure may contain the ligand that is not in its most favorable conformation.

To narrow down the potential factors defining the formation of ACs in those 18 cases, we first investigated the effect of entropy change to the relative ligand ordering. The entropy of binding ($-T\Delta S$) for those 18 cliff pairs was computed using an empirically derived protocol as described in the Supporting Information Section S2. As the ligands involved in each AC are structurally identical with >80% similarity, the overall contribution from the entropy change is found to be relatively small (−4.9 to 2.9 kcal/mol; Table S4). More importantly, the ordering of the cliff partner changed in only one case (2PHB vs 2VWM) when the contribution from the $-T\Delta S$ was included in the total binding energy.

To determine if the observed incorrect assignment of the cliff partner has resulted from the so-far approximated protein desolvation energy, we computed the full solvation energy of protein−ligand binding at the B97-D3BJ/6-31+G(d) level of theory using SMD implicit solvation model. Note that these implicit solvation calculations on such molecules with >1000 atoms are substantially more expensive than our approximate approach of calculating only the ligand desolvation energy. Though the inclusion of full solvation energy of binding improved the overall binding energy by a significant amount (by 25−50 kcal/mol), it changed the relative ordering in only three of the 18 examined ligand pairs (Table S5). This analysis suggests that the origin of error in the majority of the failed cases could be from some other effect such as the problem in the crystal structure itself.

Regarding the possibility of having issues with the crystal structures, it is important to note that we have already performed the structure minimization with 0.5 Å restraint (see method section for details) using the Amber10:EHT forcefield, which is expected to minimize most of the crystal structure-related errors. To examine the possibility of not having the ligand in its fully relaxed form in the binding pocket, we took the restraint-minimized geometry and performed a full geometry optimization of the ligand at the PM6-D3 level while keeping the protein fixed. Interestingly, using the protein−ligand complex with the

https://dx.doi.org/10.1021/acs.jcim.9b01123
J. Chem. Inf. Model. XXXX, XXX, XXX−XXX

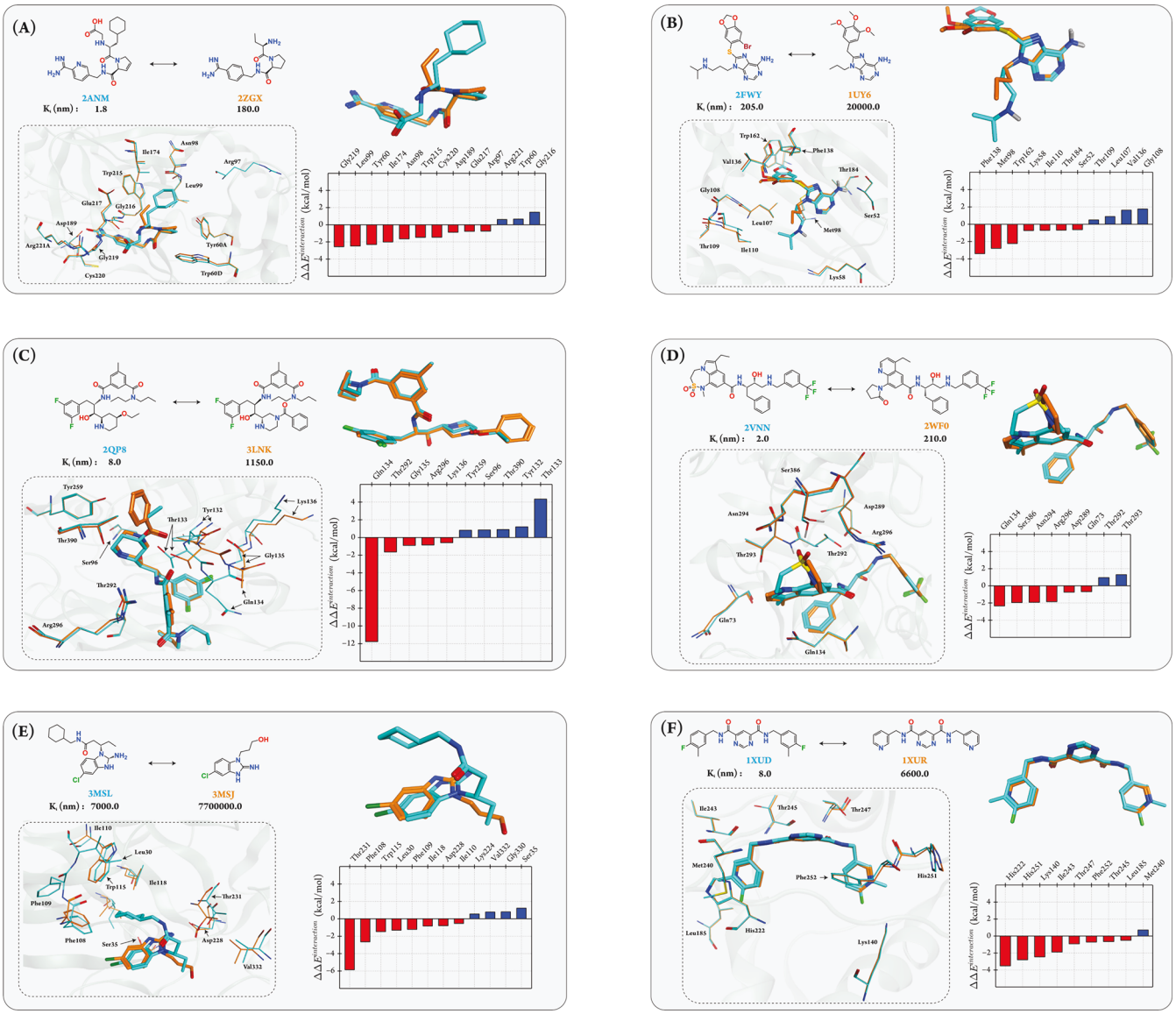

Figure 6. Difference interaction energy analysis results of some selected examples of ACs where Glide score is found to incorrectly identify the most potent ligand of the cliff. Only the residues contributing $\Delta\Delta E^{\text{interaction}}$ more than |±0.5| kcal/mol to the total interaction energy difference are shown along with their quantitative contributions. In (A–F), the most potent ligand and its receptor is shown in cyan color, whereas the other complex is shown in orange color. Receptors: (A) prothrombin, (B) heat shock protein HSP 90-alpha, (C–E) BACE1, and (F) collagenase 3.

fully optimized ligand in the binding pocket, we found the relative ordering is corrected in 4 of those 18 cliff pairs (Table S6). In the other 14 cliffs, the relative ligand ordering remained incorrect.

As the amino acid residues and ligand could be charged at the physiological pH, it is also possible that the false assignment of the AC could also stem from neutralizing the molecule in our protocol. To test if that is the case, we computed the interaction energies of a total of 46 AC pairs having a net difference in formal charge on the ligands using MIM2 protocol and SMD implicit solvation. In 42 of the 46 evaluated cases, the relative ordering of the ligand remained identical with our previous assignment using the charge−neutral systems (see Supporting Information table S7). For the remaining four cases, the ordering of the ligand changed compared to the order calculated using the charge-neutralized protocol. Interestingly, three of those four cases were among the 18 incorrectly assigned cases with our charge-neutralized protocol. This suggests that care must be taken when neutralizing the charged ligand, especially when there is a net difference in overall ligand charge. Note that some recent studies have shown that the SMD solvation model has some problems, in particular, in dealing with charged molecules.[61,62] Therefore, a more rigorous calibration of SMD implicit solvation is necessary to calibrate the accuracy.

In summary, this analysis suggests the possibility that even in the high-resolution crystal structures, the ligand may not be in its optimum binding pose and therefore resulting in an underestimation of the nonbonded interaction energies, as pointed out in some recent studies.[74] Our analysis above showed that some of those issues could be understood and corrected by systematically preparing the starting structure. Finally, other factors such as the deficiencies of our DFT methods such as BSSE, and using neutral instead of charged ligands and residues also may be responsible for some of the incorrect predictions.

https://dx.doi.org/10.1021/acs.jcim.9b01123
J. Chem. Inf. Model. XXXX, XXX, XXX−XXX

4. SUMMARY AND CONCLUSIONS

This study presents a large-scale application of QM methods in providing insight into the experimentally observed large activity differences in structurally similar ligand pairs. A set of 261 protein−ligand complexes forming a total of 205 ACs, which cover 37 different receptor types belonging to 14 different protein families, was used to assess the performance of our protocol. These cliffs were systematically identified in a previous study by Bajorath and co-workers to have at least 80% 3D similarity in ligand structure and display more than 100-fold difference in potency.[25] To lower the computational cost of high-level QM calculations (B97-D3BJ/6-311++G(3df,2p)) that are necessary to obtain reliable interaction energies, we applied our three-layer MIM (MIM3 [B97-D3BJ/6-311++G(3df,2p):B97-D3BJ/6-31+G(d):PM6-D3]) fragmentation-based approach, which accurately reproduces the high-level interaction energies at a significantly reduced computational cost. Our MIM3 approach is also shown to provide a residue-specific energy decomposition of the total interaction energy, which can be used to further analyze and identify the key residues involved in protein−ligand interactions.

In this study, we mainly focused on whether the QM binding energy calculation can correctly identify the higher potency cliff partner for a given ligand pair having a sufficiently high activity difference. We analyzed the effect of including crystal water molecules as a part of the receptor as well as the effect of ligand desolvation energy on the correct identification of the more potent ligand in a cliff pair. We found that the interaction energy contribution from all residues within 6 Å of the ligand correctly identified 77.6% (159/205) of the ACs. When the contribution from crystal water molecules was removed, the accuracy significantly improved to 86.3%. Using a simple distance and angle-based criteria, we also identified some of the unique water molecules that are essential in protein−ligand binding. Our study identified four cases where the AC is primarily formed by the bridging crystal water molecules. Additionally, we detected seven cases where the AC is formed due to the significantly large difference in ligand desolvation energies. Along with the interaction energy contribution from the unique crystal waters and ligand desolvation energy, our study correctly identified the potent cliff partner in 91.2% of the cases. These results are significantly better relative to the results from GlideScore, which correctly identified the cliff pairs in 67.8% of the cases, although the latter method is remarkably efficient.

We also employed the residue-specific difference energy analysis to identify the chemical nature of protein−ligand interaction responsible for the AC formation. We observed a large number of residues (3−20) contributed significantly (>| ±1.0| kcal/mol) to the cliff formations. In 72 of the correctly identified 3D-cliffs, the cliffs are found to be dominated by both the classical and nonclassical hydrogen bonds. Our study also identified a total of 58 cases where the lipophilic interactions were the dominant contributors. Furthermore, in 45 of the cases, the effects were somewhat mixed with non-negligible contributions from various interactions, including hydrogen-bond, lipophilic interactions, steric repulsion, and halogen bond formation.

Despite the remarkable accuracy of our protocol (91.2% correct AC prediction), there are still 18 (8.8%) cliff pairs where our protocol failed to correctly identify the AC even when high-resolution crystal structures were used along with the high-level QM calculations. The improvement from the entropy change as well as from the full solvation energy change upon protein-ligand binding was found to be minimal (only one and three cases, respectively). Interestingly, the ligand geometry optimization at the PM6-D3 level of theory corrected the ordering in 4 of those 18 failed cases. This suggests that, in addition to the accurate interaction energies, proper treatment of all components of the protein−ligand binding energy along with some additional refinement of the crystal structure, perhaps a full QM geometry optimization in solution, could further improve the results. Work in this area is underway in our group and will be addressed in the future.

■ ASSOCIATED CONTENT

Supporting Information

The Supporting Information is available free of charge at https://pubs.acs.org/doi/10.1021/acs.jcim.9b01123.

Method section for the solvation energy and entropy calculation; and data on MIM3 interaction energies (PDF)

■ AUTHOR INFORMATION

Corresponding Author

Krishnan Raghavachari − *Department of Chemistry, Indiana University, Bloomington, Indiana 47405, United States;* orcid.org/0000-0003-3275-1426; Email: kraghava@indiana.edu

Authors

Bishnu Thapa − *Department of Chemistry, Indiana University, Bloomington, Indiana 47405, United States;* orcid.org/0000-0003-3521-1062

Jon Erickson − *Lilly Research Laboratories, Eli Lilly & Company, Indianapolis, Indiana 46285, United States*

Complete contact information is available at: https://pubs.acs.org/10.1021/acs.jcim.9b01123

Notes

The authors declare no competing financial interest.

■ ACKNOWLEDGMENTS

This work was supported by Eli Lilly and Company through the Lilly Research Award Program at Indiana University. The methods used in this project were developed based on the support from the National Science Foundation grant CHE-1665427 at Indiana University. Big Red II supercomputing facility at Indiana University was used for most of the calculations in this study.

■ REFERENCES

(1) Topliss, J. *Quantitative Structure−Activity Relationships of Drugs*; Elsevier, 2012; Vol. *19*.

(2) Guha, R. On Exploring Structure−Activity Relationships. *In Silico Models for Drug Discovery*; Springer, 2013; pp 81−94.

(3) Bohacek, R. S.; McMartin, C.; Guida, W. C. The Art and Practice of Structure-Based Drug Design: A Molecular Modeling Perspective. *Med. Res. Rev.* **1996**, *16*, 3−50.

(4) Schueler-Furman, O.; Wang, C.; Bradley, P.; Misura, K.; Baker, D. Progress in Modeling of Protein Structures and Interactions. *Science* **2005**, *310*, 638−642.

(5) Coupez, B.; Lewis, R. Docking and Scoring-Theoretically Easy, Practically Impossible? *Curr. Med. Chem.* **2006**, *13*, 2995−3003.

(6) Kontoyianni, M.; Madhav, P.; Suchanek, E.; Seibel, W. Theoretical and Practical Considerations in Virtual Screening: A Beaten Field? *Curr. Med. Chem.* **2008**, *15*, 107−116.
(7) Zhang, L.; Tan, J.; Han, D.; Zhu, H. From Machine Learning to Deep Learning: Progress in Machine Intelligence for Rational Drug Discovery. *Drug Discov. Today* **2017**, *22*, 1680−1685.
(8) Leelananda, S. P.; Lindert, S. Computational Methods in Drug Discovery. *Beilstein J. Org. Chem.* **2016**, *12*, 2694−2718.
(9) Pagadala, N. S.; Syed, K.; Tuszynski, J. Software for Molecular Docking: A Review. *Biophys. Rev.* **2017**, *9*, 91−102.
(10) Lo, Y.-C.; Rensi, S. E.; Torng, W.; Altman, R. B. Machine Learning in Chemoinformatics and Drug Discovery. *Drug Discov. Today* **2018**, *23*, 1538−1546.
(11) Geppert, H.; Vogt, M.; Bajorath, J. Current Trends in Ligand-Based Virtual Screening: Molecular Representations, Data Mining Methods, New Application Areas, and Performance Evaluation. *J. Chem. Inf. Model.* **2010**, *50*, 205−216.
(12) Klambauer, G.; Hochreiter, S.; Rarey, M. Machine Learning in Drug Discovery. *J. Chem. Inf. Model.* **2019**, *59*, 945−946.
(13) Maggiora, G. M. On Outliers and Activity Cliffs − Why QSAR Often Disappoints. *J. Chem. Inf. Model.* **2006**, *46*, 1535.
(14) Huang, J.; Fan, X. Why QSAR Fails: An Empirical Evaluation Using Conventional Computational Approach. *Mol. Pharm.* **2011**, *8*, 600−608.
(15) Stumpfe, D.; Bajorath, J. Exploring Activity Cliffs in Medicinal Chemistry: Miniperspective. *J. Med. Chem.* **2012**, *55*, 2932−2942.
(16) Hu, Y.; Stumpfe, D.; Bajorath, J. Advancing the Activity Cliff Concept. *F1000Research* **2013**, *2*, 199.
(17) Stumpfe, D.; de León, A. d. l. V.; Dimova, D.; Bajorath, J. Advancing the Activity Cliff Concept, Part Ii. *F1000Research* **2014**, *3*, 75.
(18) Cruz-Monteagudo, M.; Medina-Franco, J. L.; Pérez-Castillo, Y.; Nicolotti, O.; Cordeiro, M. N. D. S.; Borges, F. Activity Cliffs in Drug Discovery: Dr Jekyll or Mr Hyde? *Drug Discov. Today* **2014**, *19*, 1069−1080.
(19) Pérez-Villanueva, J.; Méndez-Lucio, O.; Soria-Arteche, O.; Medina-Franco, J. L. Activity Cliffs and Activity Cliff Generators Based on Chemotype-Related Activity Landscapes. *Mol. Divers.* **2015**, *19*, 1021−1035.
(20) Stumpfe, D.; Hu, Y.; Dimova, D.; Bajorath, J. Recent Progress in Understanding Activity Cliffs and Their Utility in Medicinal Chemistry: Miniperspective. *J. Med. Chem.* **2013**, *57*, 18−28.
(21) Stumpfe, D.; Hu, H.; Bajorath, J. Evolving Concept of Activity Cliffs. *ACS Omega* **2019**, *4*, 14360−14368.
(22) Pennington, L. D.; Moustakas, D. T. The Necessary Nitrogen Atom: A Versatile High-Impact Design Element for Multiparameter Optimization. *J. Med. Chem.* **2017**, *60*, 3552−3579.
(23) Hussain, J.; Rea, C. Computationally Efficient Algorithm to Identify Matched Molecular Pairs (Mmps) in Large Data Sets. *J. Chem. Inf. Model.* **2010**, *50*, 339−348.
(24) Hu, X.; Hu, Y.; Vogt, M.; Stumpfe, D.; Bajorath, J. Mmp-Cliffs: Systematic Identification of Activity Cliffs on the Basis of Matched Molecular Pairs. *J. Chem. Inf. Model.* **2012**, *52*, 1138−1145.
(25) Hu, Y.; Furtmann, N.; Gütschow, M.; Bajorath, J. Systematic Identification and Classification of Three-Dimensional Activity Cliffs. *J. Chem. Inf. Model.* **2012**, *52*, 1490−1498.
(26) Furtmann, N.; Hu, Y.; Bajorath, J. Comprehensive Analysis of Three-Dimensional Activity Cliffs Formed by Kinase Inhibitors with Different Binding Modes and Cliff Mapping of Structural Analogues. *J. Med. Chem.* **2014**, *58*, 252−264.
(27) Peltason, L.; Bajorath, J. SAR Index: Quantifying the Nature of Structure− Activity Relationships. *J. Med. Chem.* **2007**, *50*, 5571−5578.
(28) de León, A. d. l. V.; Bajorath, J. Matched Molecular Pairs Derived by Retrosynthetic Fragmentation. *MedChemComm* **2014**, *5*, 64−67.
(29) Naveja, J. J.; Vogt, M.; Stumpfe, D.; Medina-Franco, J. L.; Bajorath, J. Systematic Extraction of Analogue Series from Large Compound Collections Using a New Computational Compound−Core Relationship Method. *ACS Omega* **2019**, *4*, 1027−1032.
(30) Husby, J.; Bottegoni, G.; Kufareva, I.; Abagyan, R.; Cavalli, A. Structure-Based Predictions of Activity Cliffs. *J. Chem. Inf. Model.* **2015**, *55*, 1062−1076.
(31) Méndez-Lucio, O.; Kooistra, A. J.; Graaf, C. d.; Bender, A.; Medina-Franco, J. L. Analyzing Multitarget Activity Landscapes Using Protein−Ligand Interaction Fingerprints: Interaction Cliffs. *J. Chem. Inf. Model.* **2015**, *55*, 251−262.
(32) Merz, K. M., Jr. Limits of Free Energy Computation for Protein−Ligand Interactions. *J. Chem. Theory Comput.* **2010**, *6*, 1769−1776.
(33) Raha, K.; Merz, K. M. A Quantum Mechanics-Based Scoring Function: Study of Zinc Ion-Mediated Ligand Binding. *J. Am. Chem. Soc.* **2004**, *126*, 1020−1021.
(34) Ryde, U.; Söderhjelm, P. Ligand-Binding Affinity Estimates Supported by Quantum-Mechanical Methods. *Chem. Rev.* **2016**, *116*, 5520−5566.
(35) Mucs, D.; Bryce, R. A. The Application of Quantum Mechanics in Structure-Based Drug Design. *Expert Opin. Drug Discovery* **2013**, *8*, 263−276.
(36) Gordon, M. S.; Fedorov, D. G.; Pruitt, S. R.; Slipchenko, L. V. Fragmentation Methods: A Route to Accurate Calculations on Large Systems. *Chem. Rev.* **2011**, *112*, 632−672.
(37) Watanabe, C.; Watanabe, H.; Fukuzawa, K.; Parker, L. J.; Okiyama, Y.; Yuki, H.; Yokoyama, S.; Nakano, H.; Tanaka, S.; Honma, T. Theoretical Analysis of Activity Cliffs among Benzofuranone-Class Pim1 Inhibitors Using the Fragment Molecular Orbital Method with Molecular Mechanics Poisson−Boltzmann Surface Area (Fmo+ MM-PBSA) Approach. *J. Chem. Inf. Model.* **2017**, *57*, 2996−3010.
(38) Pérez-Benito, L.; Casajuana-Martin, N.; Jiménez-Rosés, M.; van Vlijmen, H.; Tresadern, G. Predicting Activity Cliffs with Free-Energy Perturbation. *J. Chem. Theory Comput.* **2019**, *15*, 1884−1895.
(39) Mayhall, N. J.; Raghavachari, K. Molecules-in-Molecules: An Extrapolated Fragment-Based Approach for Accurate Calculations on Large Molecules and Materials. *J. Chem. Theory Comput.* **2011**, *7*, 1336−1343.
(40) Saha, A.; Raghavachari, K. Analysis of Different Fragmentation Strategies on a Variety of Large Peptides: Implementation of a Low Level of Theory in Fragment-Based Methods Can Be a Crucial Factor. *J. Chem. Theory Comput.* **2015**, *11*, 2012−2023.
(41) Thapa, B.; Beckett, D.; Jovan Jose, K. V.; Raghavachari, K. Assessment of Fragmentation Strategies for Large Proteins Using the Multilayer Molecules-in-Molecules Approach. *J. Chem. Theory Comput.* **2018**, *14*, 1383−1394.
(42) Thapa, B.; Beckett, D.; Erickson, J.; Raghavachari, K. Theoretical Study of Protein−Ligand Interactions Using the Molecules-in-Molecules Fragmentation-Based Method. *J. Chem. Theory Comput.* **2018**, *14*, 5143−5155.
(43) Thapa, B.; Raghavachari, K. Energy Decomposition Analysis of Protein−Ligand Interactions Using Molecules-in-Molecules Fragmentation-Based Method. *J. Chem. Inf. Model.* **2019**, *59*, 3474−3484.
(44) Burley, S. K.; Berman, H. M.; Bhikadiya, C.; Bi, C.; Chen, L.; Di Costanzo, L.; Christie, C.; Dalenberg, K.; Duarte, J. M.; Dutta, S.; Feng, Z.; Ghosh, S.; Goodsell, D. S.; Green, R. K.; Guranović, V.; Guzenko, D.; Hudson, B. P.; Kalro, T.; Liang, Y.; Lowe, R.; Namkoong, H.; Peisach, E.; Periskova, I.; Prlić, A.; Randle, C.; Rose, A.; Rose, P.; Sala, R.; Sekharan, M.; Shao, C.; Tan, L.; Tao, Y.-P.; Valasatava, Y.; Voigt, M.; Westbrook, J.; Woo, J.; Yang, H.; Young, J.; Zhuravleva, M.; Zardecki, C. Rcsb Protein Data Bank: Biological Macromolecular Structures Enabling Research and Education in Fundamental Biology, Biomedicine, Biotechnology and Energy. *Nucleic Acids Res.* **2018**, *47*, D464−D474.
(45) *Molecular Operating Environment (MOE)*; Chemical Computing Group ULC: 1010 Sherbooke St. West, Suite #910, Montreal, QC, Canada, H3A 2R7, 2018.
(46) Labute, P. Protonate3D: Assignment of Ionization States and Hydrogen Coordinates to Macromolecular Structures. *Proteins: Struct., Funct., Bioinf.* **2009**, *75*, 187−205.
(47) The standard Amber10 force field to describe the protein and extended Huckel theory (EHT) for the ligand to include the electronic effect.

https://dx.doi.org/10.1021/acs.jcim.9b01123
J. Chem. Inf. Model. XXXX, XXX, XXX−XXX

(48) Svensson, M.; Humbel, S.; Froese, R. D.; Matsubara, T.; Sieber, S.; Morokuma, K. ONIOM: A multilayered integrated MO + MM method for geometry optimizations and single point energy predictions. A test for Diels−Alder reactions and $Pt(P(t\text{-}bu)_3)_2 + H_2$ oxidative addition. *J. Phys. Chem.* **1996**, *100*, 19357−19363.
(49) Becke, A. D. Density-Functional Thermochemistry. V. Systematic Optimization of Exchange-Correlation Functionals. *J. Chem. Phys.* **1997**, *107*, 8554−8560.
(50) Schmider, H. L.; Becke, A. D. Optimized Density Functionals from the Extended G2 Test Set. *J. Chem. Phys.* **1998**, *108*, 9624−9631.
(51) Grimme, S.; Antony, J.; Ehrlich, S.; Krieg, H. A Consistent and Accurate Ab Initio Parametrization of Density Functional Dispersion Correction (DFT-D) for the 94 Elements H-Pu. *J. Chem. Phys.* **2010**, *132*, 154104.
(52) Grimme, S.; Ehrlich, S.; Goerigk, L. Effect of the Damping Function in Dispersion Corrected Density Functional Theory. *J. Comput. Chem.* **2011**, *32*, 1456−1465.
(53) Ditchfield, R.; Hehre, W. J.; Pople, J. A. Self-Consistent Molecular-Orbital Methods. IX. An Extended Gaussian-Type Basis for Molecular-Orbital Studies of Organic Molecules. *J. Chem. Phys.* **1971**, *54*, 724−728.
(54) Francl, M. M.; Pietro, W. J.; Hehre, W. J.; Binkley, J. S.; Gordon, M. S.; DeFrees, D. J.; Pople, J. A. Self-Consistent Molecular Orbital Methods. XXIII. A Polarization-Type Basis Set for Second-Row Elements. *J. Chem. Phys.* **1982**, *77*, 3654−3665.
(55) Hariharan, P. C.; Pople, J. A. The Influence of Polarization Functions on Molecular Orbital Hydrogenation Energies. *Theor. Chim. Acta* **1973**, *28*, 213−222.
(56) Hehre, W. J.; Ditchfield, R.; Pople, J. A. Self-Consistent Molecular Orbital Methods. XII. Further Extensions of Gaussian-Type Basis Sets for Use in Molecular Orbital Studies of Organic Molecules. *J. Chem. Phys.* **1972**, *56*, 2257−2261.
(57) Weigend, F.; Ahlrichs, R. Balanced Basis Sets of Split Valence, Triple Zeta Valence and Quadruple Zeta Valence Quality for H to Rn: Design and Assessment of Accuracy. *Phys. Chem. Chem. Phys.* **2005**, *7*, 3297−3305.
(58) Dolg, M.; Wedig, U.; Stoll, H.; Preuss, H. Energy-Adjusted Abinitio Pseudopotentials for the First Row Transition Elements. *J. Chem. Phys.* **1987**, *86*, 866−872.
(59) Stewart, J. J. P. Optimization of Parameters for Semiempirical Methods V: Modification of NDDO Approximations and Application to 70 Elements. *J. Mol. Model.* **2007**, *13*, 1173−1213.
(60) Marenich, A. V.; Cramer, C. J.; Truhlar, D. G. Universal Solvation Model Based on Solute Electron Density and on a Continuum Model of the Solvent Defined by the Bulk Dielectric Constant and Atomic Surface Tensions. *J. Phys. Chem. B* **2009**, *113*, 6378−6396.
(61) Thapa, B.; Raghavachari, K. Accurate P K a Evaluations for Complex Bio-Organic Molecules in Aqueous Media. *J. Chem. Theory Comput.* **2019**, *15*, 6025−6035.
(62) Ho, J.; Ertem, M. Z. Calculating Free Energy Changes in Continuum Solvation Models. *J. Phys. Chem. B* **2016**, *120*, 1319−1329.
(63) Frisch, M. J. T.; Schlegel, H. B.; Scuseria, G. E.; Robb, M. A.; Cheeseman, J. R.; Scalmani, G.; Barone, V.; Petersson, G. A.; Nakatsuji, H.; Li, X.; Caricato, M.; Marenich, A. V.; Bloino, J.; Janesko, B. G.; Gomperts, R.; Mennucci, B.; Hratchian, H. P.; Ortiz, J. V.; Izmaylov, A. F.; Sonnenberg, J. L.; Williams-Young, D.; Ding, F.; Lipparini, F.; Egidi, F.; Goings, J.; Peng, B.; Petrone, A.; Henderson, T.; Ranasinghe, D.; Zakrzewski, V. G.; Gao, J.; Rega, N.; Zheng, G.; Liang, W.; Hada, M.; Ehara, M.; Toyota, K.; Fukuda, R.; Hasegawa, J.; Ishida, M.; Nakajima, T.; Honda, Y.; Kitao, O.; Nakai, H.; Vreven, T.; Throssell, K.; Montgomery, J. A., Jr.; Peralta, J. E.; Ogliaro, F.; Bearpark, M. J.; Heyd, J. J.; Brothers, E. N.; Kudin, K. N.; Staroverov, V. N.; Keith, T. A.; Kobayashi, R.; Normand, J.; Raghavachari, K.; Rendell, A. P.; Burant, J. C.; Iyengar, S. S.; Tomasi, J.; Cossi, M.; Millam, J. M.; Klene, M.; Adamo, C.; Cammi, R.; Ochterski, J. W.; Martin, R. L.; Morokuma, K.; Farkas, O.; Foresman, J. B.; Fox, D. J. *Gaussian 16*, Revision-A03; Gaussian, Inc.: Wallingford, CT, 2016.
(64) Friesner, R. A.; Banks, J. L.; Murphy, R. B.; Halgren, T. A.; Klicic, J. J.; Mainz, D. T.; Repasky, M. P.; Knoll, E. H.; Shelley, M.; Perry, J. K.; Shaw, D. E.; Francis, P.; Shenkin, P. S. Glide: A New Approach for Rapid, Accurate Docking and Scoring. 1. Method and Assessment of Docking Accuracy. *J. Med. Chem.* **2004**, *47*, 1739−1749.
(65) Halgren, T. A.; Murphy, R. B.; Friesner, R. A.; Beard, H. S.; Frye, L. L.; Pollard, W. T.; Banks, J. L. Glide: A New Approach for Rapid, Accurate Docking and Scoring. 2. Enrichment Factors in Database Screening. *J. Med. Chem.* **2004**, *47*, 1750−1759.
(66) Friesner, R. A.; Murphy, R. B.; Repasky, M. P.; Frye, L. L.; Greenwood, J. R.; Halgren, T. A.; Sanschagrin, P. C.; Mainz, D. T. Extra Precision Glide: Docking and Scoring Incorporating a Model of Hydrophobic Enclosure for Protein− Ligand Complexes. *J. Med. Chem.* **2006**, *49*, 6177−6196.
(67) *Maestro, Schrödinger, Llc*, Release, S., 4; Schrödinger Inc.: New York, Ny, 2017.
(68) Sastry, G. M.; Adzhigirey, M.; Day, T.; Annabhimoju, R.; Sherman, W. Protein and Ligand Preparation: Parameters, Protocols, and Influence on Virtual Screening Enrichments. *J. Comput.-Aided Mol. Des.* **2013**, *27*, 221−234.
(69) *Schrödinger Suite 2018 Protein Preparation Wizard*, Schrödinger Release 2018.4; Epik, Schrödinger, LLC: New York, NY, 2016; Impact, Schrödinger, LLC, New York, NY, 2016; Prime, Schrödinger, LLC, New York, NY, 2018.
(70) Nittinger, E.; Gibbons, P.; Eigenbrot, C.; Davies, D. R.; Maurer, B.; Yu, C. L.; Kiefer, J. R.; Kuglstatter, A.; Murray, J.; Ortwine, D. F.; Tang, Y.; Tsui, V. Water Molecules in Protein−Ligand Interfaces. Evaluation of Software Tools and SAR Comparison. *J. Comput.-Aided Mol. Des.* **2019**, *33*, 307−330.
(71) Kearney, B. M.; Schwabe, M.; Marcus, K. C.; Roberts, D. M.; Dechene, M.; Swartz, P.; Mattos, C. Drop: Automated Detection of Conserved Solvent-Binding Sites on Proteins. *Proteins: Struct., Funct., Bioinf.* **2019**, *88*, 152.
(72) Turney, J. M.; Simmonett, A. C.; Parrish, R. M.; Hohenstein, E. G.; Evangelista, F. A.; Fermann, J. T.; Mintz, B. J.; Burns, L. A.; Wilke, J. J.; Abrams, M. L.; Russ, N. J.; Leininger, M. L.; Janssen, C. L.; Seidl, E. T.; Allen, W. D.; Schaefer, H. F.; King, R. A.; Valeev, E. F.; Sherrill, C. D.; Crawford, T. D. Psi4: An Open-Source Ab Initio Electronic Structure Program. *Wiley Interdiscip. Rev.: Comput. Mol. Sci.* **2012**, *2*, 556−565.
(73) Phipps, M. J. S.; Fox, T.; Tautermann, C. S.; Skylaris, C.-K. Energy Decomposition Analysis Approaches and Their Evaluation on Prototypical Protein−Drug Interaction Patterns. *Chem. Soc. Rev.* **2015**, *44*, 3177−3211.
(74) Xu, Z.; Zhang, Q.; Shi, J.; Zhu, W. Underestimated Noncovalent Interactions in Protein Data Bank. *J. Chem. Inf. Model.* **2019**, *59*, 3389−3399.

https://dx.doi.org/10.1021/acs.jcim.9b01123
J. Chem. Inf. Model. XXXX, XXX, XXX−XXX